

A model for the neutron resonance in $\text{HgBa}_2\text{CuO}_{4+\delta}$

X. Montiel^{1,2,*} and C.Pépin^{1,†}

¹*Institut de Physique Théorique, L'Orme des Merisiers, CEA-Saclay, 91191 Gif-sur-Yvette, France*

²*Department of Physics, Royal Holloway, University of London, Egham, Surrey TW20 0EX, United Kingdom*

(Dated: October 2, 2018)

We study the spin dynamics of the Resonant Excitonic State (RES) proposed, within the theory of an emergent $\text{SU}(2)$ symmetry, to explain some properties of the pseudo-gap phase of cuprate superconductors. The RES can be described as a proliferation of particle-hole patches with an internal modulated structure. We model the RES modes as a charge order with multiple $2\mathbf{p}_F$ ordering vectors, where $2\mathbf{p}_F$ connects two opposite side of the Fermi surface. This simple modelization enables us to propose a comprehensive study of the collective mode observed at the antiferromagnetic (AF) wave vector $\mathbf{Q} = (\pi, \pi)$ by Inelastic Neutron Scattering (INS) in both superconducting state (SC), but also in the Pseudo-Gap regime. In this regime, we show that the dynamic spin susceptibility accuses a loss of coherence terms except at special wave vectors commensurate with the lattice. We argue that this phenomenon could explain the change of the spin response shape around \mathbf{Q} . We demonstrate that the hole dependence of the RES spin dynamics is in agreement with the experimental data in $\text{HgBa}_2\text{CuO}_{4+\delta}$.

I. INTRODUCTION

Inelastic Neutron Scattering (INS) and Electronic Raman spectroscopy (ERS) are experimental probes based on two particles processes which allow the observation of coherence effects, like the superconducting (SC) coherence peak whose energy is proportional to the transition temperature T_c , or the emergence of collective modes, which act a signature of the symmetries of the system. The study of collective modes could be a key to reveal the physical mechanisms at the origin of high critical temperature SC of cuprate compounds. A long standing mystery of such compounds is the pseudo-gap (PG) phase which exists in the underdoped regime¹⁻³ (see Fig. 1) and manifests itself by a loss of electronic density of states, without being related to any obvious symmetry breaking.

The presence of a collective spin resonance around the antiferromagnetic (AF) wave vector in the SC state has been known long ago. It has first been observed by INS experiments around the AF wave vector $\mathbf{Q} = (\pi, \pi)$ at a frequency $\omega_{res} = 41 \text{ meV}$ in $\text{YBa}_2\text{Cu}_3\text{O}_{7-\delta}$ (YBCO)⁴⁻¹⁵ and at similar energies in other compounds¹⁶⁻²⁰ in the superconducting (SC) phase. In this paper, we focus our study on recent experiments performed in monolayer Hg-based cuprate compounds: $\text{HgBa}_2\text{CuO}_{4+\delta}$ (Hg-1201)²¹. This compound represents a perfect playground to study the physics of cuprates superconductors. It is a single CuO_2 layer that allows to neglect the effect of interlayer coupling of multilayered systems as well as the effect charge reservoir, such as CuO chains in YBCO or incommensurate BiO layer in $\text{Bi}_2\text{Sr}_2\text{CaCu}_2\text{O}_{o+\delta}$ (Bi-2212) compounds. It exhibits the universal resonance around the AF wave vector \mathbf{Q} , which shows three main features.

1) The resonance stands below the $2\Delta_{SC}^0$ threshold of particle-hole continuum (Δ_{SC}^0 is the maximum of the d -wave superconducting (SC) gap) and the frequency resonance ω_{res} decreases with underdoping²¹. Moreover, a precursor of this resonance exists in the PG above T_c ,

the SC critical temperature²¹ where the resonance is observed at the same frequency ω_{res} than in the SC state with a lower intensity. The latter has also been observed in other cuprate compounds^{12-15,22-24}.

2) The energy fluctuation spectrum around \mathbf{Q} has a peculiar behavior and distribution in phase space in the underdoped regime²¹. The low and high energy parts of the fluctuation spectrum behave differently with temperature. The high energy part (for $\omega \gtrsim \omega_{res}$) of the energy fluctuation spectrum does not change across T_c or T^* , the pseudo-gap (PG) critical temperature. This behavior most probably corresponds to the response of localized spins which originate the proximity of the AF phase. On the other hand, the low energy part ($\omega \lesssim \omega_{res}$) of the energy fluctuation spectrum changes across T_c . Below, T_c , a gap opens around \mathbf{Q} and the intensity of the resonance increases from T_c and $T = 0$. Moreover, two branches appear from either side of the momentum \mathbf{Q} and meet in \mathbf{Q} at $\omega = \omega_{res}$ forming the so-called X-shape- also called "hourglass"-shape. Above T_c , the gap at \mathbf{Q} closes and the two energy branches disappear, forming the so called Y-shape- while the intensity of the resonance decreases until T^* . This feature has been observed in other cuprate compounds²⁴⁻²⁸.

3) A very specific doping dependence of the spin fluctuations is reported in monolayer Hg-based cuprate compound Hg-1201²¹. In the underdoped regime, at hole doping below 0.12 ($p < 0.12$), a Y-shape has been observed close to the vector \mathbf{Q} in both the PG and the SC phase without any change at T_c . For higher doping, $p \geq 0.12$, the X-shape is recovered in the SC phase. A summary of the different features is presented in Fig.1

Several models have been proposed to explain this collective mode²⁹⁻⁴⁰. An exhaustive review of all these approaches is presented in Ref.41. Among various scenarii to account for the spin excitation spectrum in the SC state, the INS resonance was ascribed to $\text{SO}(5)$ emergent symmetry as a π -collective mode^{32,42} relating SC to AF order. However, it has been shown that the π -mode has

an anti-bounding with the optical mode which pushes it at a higher energy than experimentally observed³⁴. The most commonly accepted explanation within the framework of itinerant magnetism, is that the INS resonance is a particle-hole bound state below the spin gap (a spin-triplet exciton) which is stabilized by repulsive interaction left within the d -wave SC state.^{34–36,38–40,43,44} This scenario well reproduces the structure of the spin excitation in the SC state in the optimally and overdoped regime. In the underdoped regime, the observation of the INS resonance in the PG state above T_c leads to a more complex situation. The shape of the resonance changes from “X” to “Y” with the presence of some additional spectral weight in the vicinity of \mathbf{Q} , whereas, in Hg-1201, the energy of the collective mode remains unchanged compared to the SC phase (see Fig. 1). This observation is very difficult to account for theoretically. Recently, an incommensurate spiral spin order stabilized by quantum fluctuations upon doping the AF Mott insulator has been proposed to explain the evolution of the energy fluctuation spectrum around \mathbf{Q} with doping in YBCO⁴⁵. The main difficulties lies on a correct modelization of the PG phase which, if we believe the excitonic explanation in the SC phase, has to retain a certain amount of coherence if the collective mode is to be observed at all in this regime.

In parallel, ERS measurements in Hg-1201 provides very interesting and complementary information for the study of collective modes in the underdoped regime. A noticeable change of behavior is observed in Raman data around 0.12 hole doping. Raman scattering is a dynamical response, which probes the charge channel at $q = 0$. Moreover, specific structure factors enable to scan the Brillouin zone with respect to respective symmetries : the A_{1g} response is isotropic, the B_{1g} symmetry scans the anti-nodal (AN) regions $(0, \pm\pi)$ and $(\pm\pi, 0)$, while the B_{2g} symmetry selects the nodal (N) region $(\pm\pi/2, \pm\pi/2)$ ⁴⁶. For doping $p < 0.12$, the Raman data exhibits a large SC coherence peak in the B_{2g} symmetry, while its intensity is very low in the B_{1g} symmetry. For higher doping, $p \geq 0.12$, the SC coherent peak has a huge intensity in the B_{1g} symmetry and decreases in the B_{2g} symmetry^{47,48}. This change of behavior around the same doping in both Raman and INS probes suggests that the coherence effect that are getting lost around T_c are a key in the explanation of the feature 3). To the best of our knowledge, the feature 3) has only been observed in Hg-1201 compound.

Here, we calculate the two-particle responses in both charge and spin sectors and compare them with experimental observations reported by ERS and INS in the underdoped regime, within a new theoretical explanation for the of the PG phase : the Resonant Excitonic State (RES) which can be described as preformed excitonic (particle-hole) pairs^{49,50}. Although different theoretical approaches have been developed to explain the PG phase, as stated above, the issue of the change of shape of the INS resonance across T_c has never been

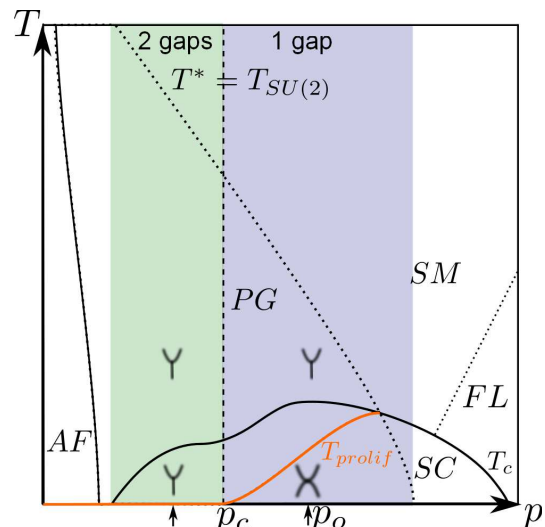


FIG. 1. (Color online) Schematic Temperature- doping (T,p) phase diagram of hole-doped cuprate compounds. The anti-ferromagnetic (AF) phase develops close to half filling ($p = 0$). The SC phase appears at intermediate hole doping and T_c is maximum at optimal doping p_o . Above T_c , in the underdoped regime, $p < p_o$, the system exhibits a large pseudo-gap (PG) phase until the temperature $T^* = T_{SU(2)}$. The RES model explains the PG phase by the proliferation of local excitonic patches above the temperature T_{prolif} (orange line)⁴⁹. The proliferation temperature vanishes below the doping p_c . Below p_c , the preformed particle hole pairs in the RES are more stable than the Cooper pairs. Consequently, the Fermi surface is fractionalized : the Cooper pairs develop in the N region only while the preformed particle-hole pairs populate in the AN region. The system exhibits a two-gap regime (green area). For doping above p_c , the particle-hole pairs are less stable than the Cooper pairs and the SC gaps out the whole Fermi surface. The system exhibits a one-gap regime (blue area). The two black arrows represent the two hole doping where further calculations are performed. left arrow) Below p_c , we have $T_{prolif} = 0$ then RES is strong compared to SC and the AN region is massively gapped by RES mechanism and $\Delta_{RES} > \Delta_{SC}$ in the AN region of the first BZ. It is a two-gaps regime and the energy fluctuation spectrum of the spin susceptibility exhibits the same Y-shape in both the PG and the SC phase. right arrow) Close to optimal doping (for $p_c < p$), we have $T_{prolif} \neq 0$. The RES is weaker than SC state and $\Delta_{RES} < \Delta_{SC}$ in the AN region of the first BZ. Consequently in the SC state, the AN zone is nearly completely gapped out by Cooper pairs. It is a one-gap regime where the energy fluctuation spectrum exhibit a X-shape in the SC phase which transforms itself in a Y-shape above T_c .

addressed before and a comprehensive study of the relations between neutron and Raman susceptibilities in this region are given here for the first time. There have been many proposals for the PG phase of the cuprates, based on AF fluctuations^{51–53}, strong correlations^{54–56}, loop current^{57,58} or emergent symmetry models^{42,59}. A recent study proposes explain the PG phase with a $SU(2)$ emergent symmetry model where the $SU(2)$ symmetry relates the SC state to the charge sector^{60,61}. The PG

phase is then described by a composite d -wave SC and charge order parameter and the SU(2) symmetry is restored by thermal fluctuations^{60,61}.

Recent investigations demonstrated that SU(2) symmetry could emerge from short-range AF interactions^{49,50}. Proceeding by integrating out the SU(2) pairing fluctuations, we describe the PG state as a new type of charge order called Resonant Excitonic State (RES)^{49,50}. The RES can be described as excitonic (particle-hole pair) patches with an internal checkerboard charge modulation. In this scenario, the PG originates SU(2) pairing fluctuations and the whole physics in the underdoped regime is governed by SU(2) symmetry. Such a scenario naturally associates the resonance observed in the PG phase with the underlying SU(2) symmetry. The novelty of our approach is that a certain form of coherence is retained in the PG phase, at specific wave vector commensurate with the lattice. The role of the underlying SU(2) symmetry is essential here in two ways. It preferentially selects a d -wave form factor for the pseudo-gap, thus allowing a change of sign between anti-nodal $(0, \pm\pi)$ and $(\pm\pi, 0)$ regions related by the vector \mathbf{Q} . It also restricts the gapping out of the Fermi surface to a small region around the anti-nodes, which leads to the emergence of spectral weight around \mathbf{Q} . The specific ‘‘Y’’ shape of the resonance in the PG phase, with the elongated tail at \mathbf{Q} is specific, within our theory, of the particle-hole excitons with many $2\mathbf{p}_F$ wave vectors.

This paper is divided as follow : in the section II, we present the theoretical model we have used to model the RES and the SC state and we explain how we calculate the spin susceptibility and the Raman susceptibility. In section III, we present our results. In the section IV, we present a discussion of our results and a comparison with the experimental data before to conclude in the section V.

II. THE THEORETICAL MODEL

In this section, we present the minimal model that describes the Resonant Excitonic State (RES). The RES is a recent scenario proposed to explain the PG phase^{49,50}.

In this model, we modelize the RES as a charge ordering state with multiple $2\mathbf{p}_F$ ordering vectors. The $2\mathbf{p}_F$ vectors connect two opposite sides of the Fermi surface (see Fig. 2). The $2\mathbf{p}_F$ vectors depend on the momentum \mathbf{k} in the first BZ and write as a function of momentum \mathbf{k} : $2\mathbf{p}_F(\mathbf{k})$. In the following, we assume that the $2\mathbf{p}_F$ vector of a point far from the Fermi surface is the $2\mathbf{p}_F$ vector of the closest point of the Fermi surface. Note that on the Fermi surface, we have $2\mathbf{p}_F(\mathbf{k}_F) = -2\mathbf{k}_F$ which implies that $\mathbf{k}_F - 2\mathbf{p}_F(\mathbf{k}_F) = -\mathbf{k}_F$. The vectors $2\mathbf{p}_F(\mathbf{k})$ are represented in Fig. 2. The $2\mathbf{p}_F$ structure corresponds to charge modulations with multiple wave vectors, which creates local modes, also called ‘‘patches’’ or ‘‘droplets’’ of

particle-hole pairs.

Here we study how the proliferation of those modes can account, phenomenologically, for the INS spectrum around \mathbf{Q} in the SC and in the PG phases, where the PG phase is described by a RES, in competition with the SC phase. At low temperature, SC and RES coexist until T_c , forming a kind of super solid. Moreover the proliferation temperature for the local RES modes is doping dependent, as depicted as the orange line in Fig.1. For $p < 0.12$, the proliferation temperature is extremely small, meaning that the whole AN region of the BZ is dominated by the RES, and the superconductivity comes mainly from the region around the nodes. For $0.12 < p < 0.25$ the proliferation temperature is non zero, which means that at low temperature we are inside a ‘‘one gap’’ SC phase. Above T_c until T^* only the RES remains^{49,50}.

An important point, in our scenario, is that the binding force leading to the formation of the particle-hole pairs, is the SU(2) fluctuations between the SC state and the charge sectors. While these fluctuations are gapped in the SC phase, they become important in the PG phase and in the underdoped region, which leads to the formation, and proliferation of patches - or droplets- of excitonic particle-hole pairs above a characteristic temperature, here T_{prolif} .

A. The RES minimal model

The simplified version of our theory consists of performing a mean field decoupling of a Hamiltonian retaining short range AF correlations in the charge and SC channels.

$$\mathcal{H}_{start} = \sum_{i,j,\sigma} t_{ij} c_{i\sigma}^\dagger c_{j\sigma} + \frac{1}{2} \sum_{\langle i,j \rangle} J_{ij} \mathbf{S}_i \cdot \mathbf{S}_j, \quad (1)$$

where t_{ij} is the hopping from site i to j and J_{ij} the AF super-exchange between spins $\mathbf{S}_i = \sum_{\alpha\beta} c_{i\alpha}^\dagger \vec{\sigma}_{\alpha\beta} c_{i\beta}$ sitting on nearest neighbors $\langle i,j \rangle$ ^{31,62}. $\vec{\sigma}_{\alpha\beta}$ is a set of Pauli Matrices and $c_{i,\sigma}^{(\dagger)}$ is the annihilation (creation) operator of an electron with the spin σ on site i . Note that the effects of strong on-site Coulomb repulsion and thus the double occupancy, are so far neglected in this model. Applying the Fourier transform on the fermionic operator $c_{i,\sigma} = \frac{1}{\sqrt{N}} \sum_{\mathbf{k}} c_{\mathbf{k},\sigma} e^{i\mathbf{k}\cdot\mathbf{r}_i}$, the Hamiltonian in Eq. (1) becomes :

$$\mathcal{H}_{start} = \sum_{\mathbf{k},\sigma} \xi_{\mathbf{k}} c_{\mathbf{k}\sigma}^\dagger c_{\mathbf{k}\sigma} + \frac{1}{2} \sum_{\mathbf{k},\mathbf{k}',\mathbf{q}} J_{\mathbf{q}} c_{\mathbf{k}\alpha}^\dagger \vec{\sigma}_{\alpha\beta} c_{\mathbf{k}+\mathbf{q}\beta} c_{\mathbf{k}'+\mathbf{q}\gamma}^\dagger \vec{\sigma}_{\gamma\delta} c_{\mathbf{k}'\delta}. \quad (2)$$

We describe the RES and SC state by the effective action $S_{\text{eff}} = -\sum_{\mathbf{k},\sigma} \Psi_{\mathbf{k}}^\dagger \hat{G}^{-1} \Psi_{\mathbf{k}}$, in the basis $\Psi_{\mathbf{k}}^\dagger = (c_{\mathbf{k},\sigma}^\dagger, c_{-\mathbf{k}+2\mathbf{p}_F(-\mathbf{k}),\bar{\sigma}}, c_{\mathbf{k}+2\mathbf{p}_F(\mathbf{k}),\sigma}, c_{-\mathbf{k},\bar{\sigma}})$, and with

$$\hat{G}^{-1}(\mathbf{k}, \epsilon) = \begin{pmatrix} i\epsilon - \xi_{\mathbf{k}} & 0 & \Delta_{RES,\mathbf{k}} & \Delta_{SC,\mathbf{k}} \\ 0 & i\epsilon + \xi_{-\mathbf{k}+2\mathbf{p}_F(-\mathbf{k})} & \Delta_{SC,\mathbf{k}+2\mathbf{p}_F(\mathbf{k})}^\dagger & -\Delta_{RES,\mathbf{k}} \\ \Delta_{RES,\mathbf{k}}^\dagger & \Delta_{SC,\mathbf{k}+2\mathbf{p}_F(\mathbf{k})} & i\epsilon - \xi_{\mathbf{k}+2\mathbf{p}_F(\mathbf{k})} & 0 \\ \Delta_{SC,\mathbf{k}}^\dagger & -\Delta_{RES,\mathbf{k}} & 0 & i\epsilon + \xi_{-\mathbf{k}} \end{pmatrix}. \quad (3)$$

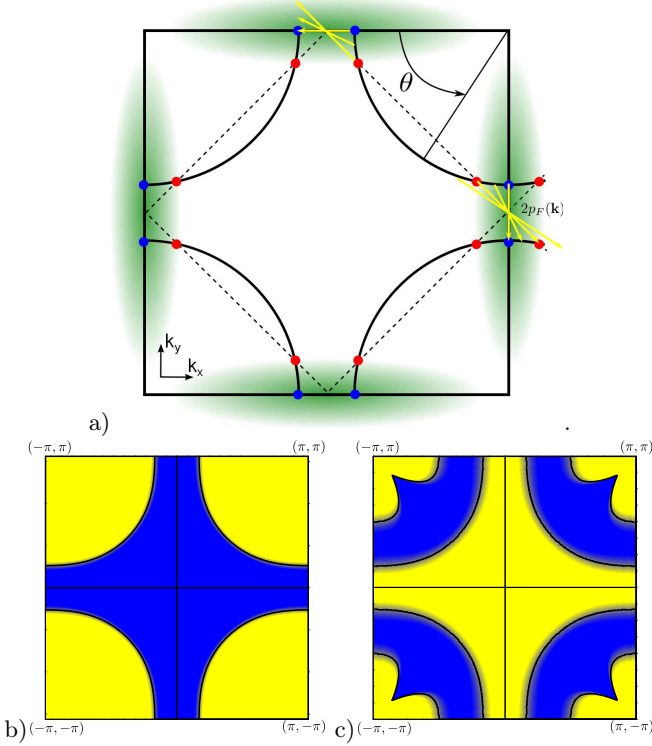


FIG. 2. (Color online) a) Schematic representation of the hole-doped Fermi surface (solid line) in first Brillouin zone of the square lattice. The angle θ localizes the point on the FS. The values $\theta = 0$ and $\pi/2$ represent the AN-zone while $\theta = \pi/4$ stands for the N zone of the first BZ. The magnetic BZ is presented in dashed line while its intersections with the Fermi surface (the hot-spots) are the red points. The yellow arrows represent the $2\mathbf{p}_F$ ordering vectors in the Anti-Nodal (AN) region. Note $2\mathbf{p}_F$ vector depends on the momentum \mathbf{k} . The RES gap develops in the AN zone (green area). The point of the FS at the zone edge are drawn in blue circles. In b) we represent the bare electronic dispersion $\xi_{\mathbf{k}}$ at optimal doping $p = 0.16$ while in c) we represent the $2\mathbf{p}_F$ -shifted electronic dispersion $\xi_{\mathbf{k}+2\mathbf{p}_F(\mathbf{k})}$. The blue (yellow) area shows the electron (hole) states that have negative (positive) energy separated by the Fermi surface (solid line). Note that the FS of the bare and the $2\mathbf{p}_F$ -shifted electronic dispersions are the same whereas the curvature close to the FS is reversed.

Here $\xi_{\mathbf{k}}$ is the electron dispersion, including the chemical potential μ with $\xi_{-\mathbf{k}} = \xi_{\mathbf{k}}$ and ϵ is the fermionic Matsubara frequency. $\Delta_{SC,\mathbf{k}}$ is the superconducting order parameter and $\Delta_{RES,\mathbf{k}}$ the RES one, which couples $\mathbf{k} \rightarrow \mathbf{k} - 2\mathbf{p}_F(\mathbf{k})$. The RES order parameter describes the particle-hole pairs patches that break locally

the translational symmetry⁵⁰. We use a tight-binding description of the electronic spectrum of Hg-1201 with $\xi_{\mathbf{k}} = -2t_1(\cos(k_x a) + \cos(k_y a)) + 2t_2 \cos(k_x a) \cos(k_y a) + t_3(\cos(2k_x a) + \cos(2k_y a)) + t_4(\cos(2k_x a) \cos(k_y a) + \cos(k_x a) \cos(2k_y a)) - \mu$ where t_i are the i^{th} neighbor hopping parameters. We have $t_1 = -0.408 \text{ eV}$, $t_2 = 0.093 \text{ eV}$, $t_3 = 0.071 \text{ eV}$ and $t_4 = 0.036 \text{ eV}$ (deduced from ab-initio calculations⁶³) which gives a bandwidth of 1.5 eV . a is the elementary cell parameter set to unity $a = 1$ and μ is the chemical potential adjusted to determine the hole doping. The Fermi surfaces of the spectrum $\xi_{\mathbf{k}}$ and $\xi_{\mathbf{k}+2\mathbf{p}_F(\mathbf{k})}$ are presented on the figure 2. Note that the bandwidth of the spectrum $\xi_{\mathbf{k}}$ is larger than the bandwidth of the spectrum $\xi_{\mathbf{k}+2\mathbf{p}_F(\mathbf{k})}$. We determined the Green's functions of the model by inverting the matrix (3)

As highlighted in previous studies^{49,50}, the interplay of the SC and the RES order parameters is not trivial. For intermediate temperature ($T_c < T < T^*$), only RES remains in the system. The RES leads to the opening of a gap in the AN zone of the first BZ, and the formation of Fermi arcs^{49,50}. We consider a RES order parameter with a d -wave symmetry as it is the SU(2) partner of the d -wave SC state :

$$\Delta_{RES,\mathbf{k}} = \frac{\Delta_{RES}^0}{2} \gamma_{\mathbf{k}} e^{\left(-\frac{(k_x - \pi)^2 a^2}{2\sigma_x^2} - \frac{(k_y)^2 a^2}{2\sigma_y^2} \right)}, \quad (4)$$

with $\gamma_{\mathbf{k}} = (\cos(k_x a) - \cos(k_y a))$.

Here $\sigma_{x(y)}$ is the width of the Gaussian function in the $k_x(k_y)$ direction (see Fig. 2). This parametrization has been used to explain the opening of the PG and the formation of Fermi arcs observed by Angle Resolved PhotoEmission Spectroscopy (ARPES)⁶⁴.

Below T_c ($T < T_c$), we define a d -wave gap envelop $C_{\mathbf{k}}$ which will take into account the coexistence between the SC state and the RES. The definition of the RES order parameter is the same than above T_c (see relation 4). In the following we assume that the gap envelop is related to the SC and the RES order parameters by the relation:

$$C_{\mathbf{k}} = \sqrt{\Delta_{SC,\mathbf{k}}^2 + \Delta_{RES,\mathbf{k}}^2}, \quad (5)$$

where $C_{\mathbf{k}}$ has a d -wave symmetry and a magnitude C^0 : $C_{\mathbf{k}} = \frac{C^0}{2} \gamma_{\mathbf{k}}$. Considering, the relation (5), we can deduce the form of the SC order parameter, $\Delta_{SC,\mathbf{k}} = \sqrt{C_{\mathbf{k}}^2 - \Delta_{RES,\mathbf{k}}^2}$. The variation of the SC and RES order

parameters in the SC phase along the Fermi surface is presented in the Figs. 4 and 5. The RES develops solely in the AN zone of the first BZ (see relation 4) while the superconducting state can exist both in the nodal and anti-nodal zones. This momentum dependence of the SC and the RES order parameters in the first BZ is supported by electronic Raman Scattering experiments in Hg-1201^{47,48} or Bi-2212⁶⁵ compounds as well as ARPES experiments^{66,67}. The resolution of the self-consistency equation deriving from the minimal model is left for a forthcoming publication. In the following, we determine the value of the gap magnitude that reproduce the experimental data.

The real space picture is that the RES is formed of local objects, patches or droplets, which compete with the global SC phase. When temperature is raised, the entropy associated with the local object is always winning compared to the energy of the global phase, in analogy with the proliferation of vortices in a stiff quantum fluid⁶⁸. Hence there exists a proliferation temperature for the patches of excitons, which can be understood as follows. When the binding energy for the formation of the Cooper pairs is greater than the energy for the formation of the particle hole pairs, the proliferation occurs above a certain temperature $T_{prolif} \simeq (E_{CP}^2 - E_{EP}^2)/g$, where E_{CP} and E_{EP} is the mean field scale for the formation of Cooper and particle-hole pairs (at $2\mathbf{p}_F$), respectively and g is a coupling constant coming from a simple Ginzburg Landau treatment⁴⁹. On the other hand, when $E_{CP} < E_{EP}$, then the proliferation of exciton droplets starts at very low temperature, which leads to $T_{prolif} \simeq 0$. For a simple discussion, we identify $E_{CP} \simeq T_c$ while $E_{EP} \simeq T_{SU(2)}$, which is the energy scale associated to the SU(2) fluctuations in our theory^{49,50}. As depicted in Fig.1, there is a critical doping p_c , situated in the underdoped region, below which $T_{prolif} \simeq 0$, whereas for $p > p_c$, $T_{prolif} \neq 0$. The critical doping p_c is a crucial ingredient of our theory to explain the experimental data in Hg-1201.

B. The spin susceptibility

We turn to the evaluation of the spin susceptibility in the SC state and the RES. In the SC phase, we expect

the spin-exciton process that explains the spin dynamics in the overdoped part of the cuprate phase diagram to be strongly affected by the emergence of RES in the underdoped part of the phase diagram. The spin operator writes $S_{\mathbf{q}} = \frac{1}{\sqrt{N}} \sum_{\mathbf{k}} c_{\mathbf{k},-\sigma}^\dagger c_{\mathbf{k}+\mathbf{q},\sigma}$ which destroy a bosonic excitations at momentum \mathbf{q} with a charge 0 and spin 1. Rewriting the Hamiltonian Eq. (2) with the spin operator, we get $\mathcal{H}_{start} = \sum_{\mathbf{k},\sigma} \xi_{\mathbf{k}} c_{\mathbf{k}\sigma}^\dagger c_{\mathbf{k}\sigma} + \frac{1}{2} \sum_{\mathbf{q}} J_{\mathbf{q}} S_{\mathbf{q}}^\dagger S_{\mathbf{q}}$. The spin susceptibility is derived from the linear response of the spin operator and reads $\chi_S = -i\theta(t) \langle S_{\mathbf{q}}^\dagger(t) S_{\mathbf{q}}(0) \rangle$. Within the Random Phase Approximation (RPA), the full spin susceptibility writes :

$$\chi_S(\omega, \mathbf{q}) = \frac{\chi_S^0(\omega, \mathbf{q})}{1 + J(\mathbf{q})\chi_S^0(\omega, \mathbf{q})} \quad (6)$$

with $J(\mathbf{q}) = 2J_0(\cos(q_x a) + \cos(q_y a))$ due to exchange between near-neighbor copper sites. In the equation (6), χ_S^0 is the bare polarization bubble constructed from the Green's function and $J(\mathbf{q})$ is super-exchange interaction from Eqn.(1). Note that full diagrammatic contributions to the bare susceptibility is discussed in Appendix A. The bare polarization can be evaluated by the formula^{33,69}:

$$\chi_S^0(\omega, \mathbf{q}) = -\frac{T}{2} \sum_{\epsilon, \mathbf{k}} \text{Tr} \left[\hat{G}(\omega + \epsilon, \mathbf{k} + \mathbf{q}) \hat{G}(\epsilon, \mathbf{k}) \right] \quad (7)$$

where $\epsilon(\omega)$ is the fermionic (bosonic) Matsubara frequency, \mathbf{k}, \mathbf{q} are the impulsions, T the temperature and Tr means Trace of the Green function matrix \hat{G} deduced from Eq. (3). Using the relation (7) we describe the spin dynamics in pure RES, pure SC phase and coexisting SC-RES phases.

1. The bare spin susceptibility in the SC phase

In the pure d -wave SC state, the bare susceptibility writes^{33,69}:

$$\begin{aligned} \chi_{S,sc}^0(\omega, \mathbf{q}) = & \sum_{\mathbf{k}} \left[\frac{1}{2} \left(1 + \frac{\xi_{\mathbf{k}} \xi_{\mathbf{k}+\mathbf{q}} + \Delta_{SC,\mathbf{k}} \Delta_{SC,\mathbf{k}+\mathbf{q}}}{E_{\mathbf{k}} E_{\mathbf{k}+\mathbf{q}}} \right) \frac{n_F(E_{\mathbf{k}+\mathbf{q}}) - n_F(E_{\mathbf{k}})}{\omega + i\eta - (E_{\mathbf{k}+\mathbf{q}} - E_{\mathbf{k}})} \right. \\ & + \frac{1}{4} \left(1 - \frac{\xi_{\mathbf{k}} \xi_{\mathbf{k}+\mathbf{q}} + \Delta_{SC,\mathbf{k}} \Delta_{SC,\mathbf{k}+\mathbf{q}}}{E_{\mathbf{k}} E_{\mathbf{k}+\mathbf{q}}} \right) \frac{1 - n_F(E_{\mathbf{k}+\mathbf{q}}) - n_F(E_{\mathbf{k}})}{\omega + i\eta + (E_{\mathbf{k}+\mathbf{q}} + E_{\mathbf{k}})} \\ & \left. + \frac{1}{4} \left(1 - \frac{\xi_{\mathbf{k}} \xi_{\mathbf{k}+\mathbf{q}} + \Delta_{SC,\mathbf{k}} \Delta_{SC,\mathbf{k}+\mathbf{q}}}{E_{\mathbf{k}} E_{\mathbf{k}+\mathbf{q}}} \right) \frac{n_F(E_{\mathbf{k}+\mathbf{q}}) + n_F(E_{\mathbf{k}} - 1)}{\omega + i\eta - (E_{\mathbf{k}+\mathbf{q}} + E_{\mathbf{k}})} \right], \quad (8) \end{aligned}$$

where $E_{\mathbf{k}} = \sqrt{\xi_{\mathbf{k}}^2 + \Delta_{SC,\mathbf{k}}^2}$ describes the SC excitations

spectrum and n_F is the Fermi-Dirac statistic. The d -

wave form factor of the SC-order parameter implies that the coherence factor is maximal on the Fermi surface. The imaginary part of the bubble exhibits a discontinuity at certain threshold, and coincidentally the real part shows a logarithmic divergence. This observation alone enables us to explain in a self consistent way the formation of the triplet collective mode. Indeed, below this energy threshold, the divergence in the real part of the spin polarization cannot be screened by the imaginary part (which vanishes below the threshold), hence leading to the emergence of the collective mode. The value of the threshold is expected to be $2|\Delta_{SC}(\mathbf{k}_{HS})|$ the factor 2 coming from the Green's functions in the bubble, where \mathbf{k}_{HS} is the momentum of the hotspots. The latter divergence guarantees the emergence of a collective mode below threshold. In order to explain the emergence of a collective mode at \mathbf{Q} , the coherent factors have to be

non zero at the Fermi surface while the FS is gapped. This condition can be fulfilled if we consider a d -wave SC state³³. This description well reproduces the imaginary part of the dynamic spin susceptibility inside the SC state in the overdoped case^{33,41}, with in particular, the ‘‘X-shape’’ form of the dispersion of the modes around (π, π) correctly given in shape and energy within this simple model. Further we consider that this model gives a good description of the phenomenon and focus on its generalization to the PG state.

2. The bare spin susceptibility in the RES

In our theory for the PG state, we evaluate the spin susceptibility in the RES. The bare spin susceptibility in the RES writes⁶⁹:

$$\chi_{S,RES}^0(\omega, \mathbf{q}) = \sum_{\mathbf{k}} \left[\frac{1}{4} \left(1 + \frac{(\xi_{\mathbf{k}} - \xi_{\mathbf{k}+2\mathbf{p}_F(\mathbf{k})})(\xi_{\mathbf{k}+\mathbf{q}} - \xi_{\mathbf{k}+\mathbf{q}+2\mathbf{p}_F(\mathbf{k}+\mathbf{q})}) + 4\Delta_{RES,\mathbf{k}}\Delta_{RES,\mathbf{k}+\mathbf{q}}f(\mathbf{q})}{(W_{+,\mathbf{k}} - W_{-,\mathbf{k}})(W_{+,\mathbf{k}+\mathbf{q}} - W_{-,\mathbf{k}+\mathbf{q}})} \right) \right. \\ \left. \left(\frac{n_F(W_{-,\mathbf{k}}) - n_F(W_{-,\mathbf{k}+\mathbf{q}})}{\omega + i\eta + W_{-,\mathbf{k}} - W_{-,\mathbf{k}+\mathbf{q}}} + \frac{n_F(W_{+,\mathbf{k}}) - n_F(W_{+,\mathbf{k}+\mathbf{q}})}{\omega + i\eta + W_{+,\mathbf{k}} - W_{+,\mathbf{k}+\mathbf{q}}} \right) \right. \\ \left. + \frac{1}{4} \left(1 - \frac{(\xi_{\mathbf{k}} - \xi_{\mathbf{k}+2\mathbf{p}_F(\mathbf{k})})(\xi_{\mathbf{k}+\mathbf{q}} - \xi_{\mathbf{k}+\mathbf{q}+2\mathbf{p}_F(\mathbf{k}+\mathbf{q})}) + 4\Delta_{RES,\mathbf{k}}\Delta_{RES,\mathbf{k}+\mathbf{q}}f(\mathbf{q})}{(W_{+,\mathbf{k}} - W_{-,\mathbf{k}})(W_{+,\mathbf{k}+\mathbf{q}} - W_{-,\mathbf{k}+\mathbf{q}})} \right) \right. \\ \left. \left(\frac{n_F(W_{-,\mathbf{k}}) - n_F(W_{+,\mathbf{k}+\mathbf{q}})}{\omega + i\eta + W_{-,\mathbf{k}} - W_{+,\mathbf{k}+\mathbf{q}}} + \frac{n_F(W_{+,\mathbf{k}}) - n_F(W_{-,\mathbf{k}+\mathbf{q}})}{\omega + i\eta + W_{+,\mathbf{k}} - W_{-,\mathbf{k}+\mathbf{q}}} \right) \right], \quad (9)$$

where $W_{\pm,\mathbf{k}} = \frac{1}{2} \left(\xi_{\mathbf{k}} + \xi_{\mathbf{k}+2\mathbf{p}_F(\mathbf{k})} \pm \sqrt{(\xi_{\mathbf{k}} - \xi_{\mathbf{k}+2\mathbf{p}_F(\mathbf{k})})^2 + 4\Delta_{RES,\mathbf{k}}^2} \right)$ is the RES excitations spectrum and $f(\mathbf{q})$ a function of momentum \mathbf{q} that takes into account the coherence conditions of the RES, as detailed further in the text and in Appendix A.

The contribution to the bare spin susceptibility in the RES (equation (9)) can be divided in two parts : the intraband contribution (upper terms in relation (9)) and the interband contribution (lower terms in the relation (9)). Close to $\mathbf{q} = \mathbf{Q}$, the intraband contribution can be neglected and the whole signal is produced by interband processes. As the FS formed by the hybridized bands cannot be connected by the vector \mathbf{Q} , the bare spin susceptibility is gapped up to the energy $2|\Delta_{RES}(\mathbf{k}_{HS})|$. Far from $\mathbf{q} = \mathbf{Q}$, the intraband processes become non negligible.

Deeper investigation on the SU(2) symmetry have shown that the SU(2) pairing fluctuations emerging from non-linear σ model only exist in a restricted area $S_{\mathbf{k}}$ in the AN part of the first BZ (see Ref.⁴⁹ for the detailed demonstration and particularly the figure 9 where $S_{\mathbf{k}}$ is represented). In the following, one important element is that we assume a symmetrization of this restricted area between two adjacent AN area (in \mathbf{k} and $\mathbf{k} + \mathbf{Q}$ with $\mathbf{Q} = (\pi, \pi)$) such that $S_{\mathbf{k}} = S_{\mathbf{k}+\mathbf{Q}}$.

The coherence terms are described by the Feynman di-

agram shown in Fig. 3 a) and we observe that the outgoing vector of the Feynman diagram does not equal the incoming vector \mathbf{q} up to the difference $\bar{\delta}_{2\mathbf{p}_F} = 2\mathbf{p}_F(\mathbf{k} + \mathbf{q}) - 2\mathbf{p}_F(\mathbf{k})$. The difference $\bar{\delta}_{2\mathbf{p}_F}$ vanishes ($\bar{\delta}_{2\mathbf{p}_F} = \mathbf{0}$) only if \mathbf{q} is commensurate and differs from zero ($\bar{\delta}_{2\mathbf{p}_F} \neq \mathbf{0}$) for incommensurate \mathbf{q} vectors (see Fig. 3). Consequently the coherence terms exist only close $\mathbf{q} = \mathbf{0}, \mathbf{Q}$ and cannot exist far from commensurate vectors. In the following, we modelize the RES coherence terms in Eq. (9) by the terms $\Delta_{RES,\mathbf{k}}\Delta_{RES,\mathbf{k}+\mathbf{q}}f(\mathbf{q})$ where $f(\mathbf{q})$ vanishes for incommensurate \mathbf{q} vectors. More precisely, the function $f(\mathbf{q})$ equals one around $\mathbf{q} = \mathbf{0}$ and $\mathbf{q} = \mathbf{Q}$ and vanishes for other vectors. A full description of the function $f(\mathbf{q})$ is done in the appendix A while the effect of the function $f(\mathbf{q})$ on the spin susceptibility is studied in appendix B.

In contrast to the preformed Cooper pair scenario³³ we observe a resurgence of the coherence terms around incoming wave vectors commensurate with the lattice, like $\mathbf{q} = \mathbf{Q}$. In the RES scenario, the coherence terms only exist close to commensurate \mathbf{q} vectors. This peculiar behavior is different from the scenario of preformed Cooper

pairs where the coherence terms vanish for all \mathbf{q} vectors.

Close to the FS, we can linearize the shifted spectrum $\xi_{\mathbf{k}-2\mathbf{p}_F(\mathbf{k})}$. This linearization leads to the relation $\xi_{\mathbf{k}-2\mathbf{p}_F(\mathbf{k})} \approx -\xi_{\mathbf{k}}$ only valid close to the FS. In this approximation, the relation (9) is equal to the relation (8). We can deduce that the low energy spectrum in the RES and the SC state are nearly the same.

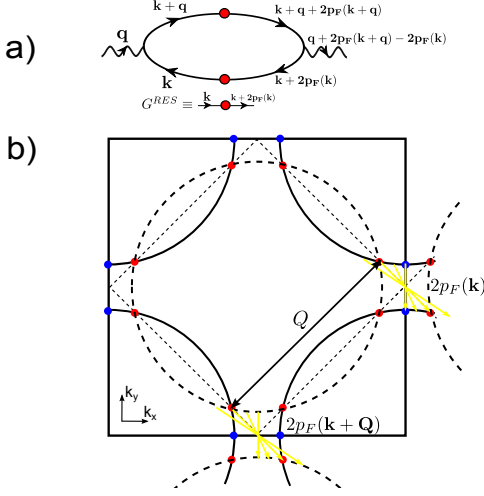


FIG. 3. (Color online) a) Diagrammatic contribution that describes the coherence between two particle-hole patches. The outgoing vector depends on the difference $2p_F(\mathbf{k} + \mathbf{q}) - 2p_F(\mathbf{k})$ which vanishes at commensurate \mathbf{q} vectors. This Feynman diagram must vanish for incommensurate \mathbf{q} vectors and exists close to commensurate \mathbf{q} vectors. b) Representation of the Fermi surface of the electrons at \mathbf{k} (solid line) and the electrons at $\mathbf{k} + \mathbf{Q}$ (dashed line). The $2p_F$ vectors of the electrons at $\mathbf{k} + \mathbf{Q}$ are the same as the electrons at \mathbf{k} (yellow arrows).

3. The bare spin susceptibility in the coexisting SC+RES phase

A detailed study of the whole Feynman diagram that contributes to the bare spin susceptibility is done in Appendix A. The main contribution of the SC and the RES state does not qualitatively change regarding the pure state study. The threshold in the bare spin susceptibility occurs at an energy $2\sqrt{\Delta_{RES}^2(\mathbf{k}_{HS}) + \Delta_{SC}^2(\mathbf{k}_{HS})}$ and depends on both SC and RES state. In addition to the RES coherent terms, note that a mixed SC+RES exists and also contributes only close to commensurate \mathbf{q} vector (see Appendix A)

C. Raman response function

The Raman Response χ_λ is the response function of a modified density operator $\chi_\lambda = -i\Theta(\tau)\langle\rho^\lambda(\tau)\rho^\lambda(0)\rangle$ with $\rho^\lambda = \sum_{\mathbf{k}} \gamma^\lambda c_{\mathbf{k}}^\dagger c_{\mathbf{k}}$ where γ^λ is the Raman vertex in

the symmetry λ ^{46,70}. The Raman susceptibility strongly depends on the symmetry of the system. We can take into account these symmetries by considering vertices in the phonon-matter interaction different from unity. In cuprates compounds, we typically study three symmetries which are written within the effective mass approximation:

$$\begin{aligned}\gamma^{B_{1g}} &= \frac{1}{2} \left[\frac{\partial^2 \xi_{\mathbf{k}}}{\partial k_x^2} - \frac{\partial^2 \xi_{\mathbf{k}}}{\partial k_y^2} \right] \\ \gamma^{B_{2g}} &= \frac{1}{2} \left[\frac{\partial^2 \xi_{\mathbf{k}}}{\partial k_x \partial k_y} + \frac{\partial^2 \xi_{\mathbf{k}}}{\partial k_y \partial k_x} \right] \\ \gamma^{A_{1g}} &= \frac{1}{2} \left[\frac{\partial^2 \xi_{\mathbf{k}}}{\partial k_x^2} + \frac{\partial^2 \xi_{\mathbf{k}}}{\partial k_y^2} \right]\end{aligned}\quad (10)$$

were the B_{1g} symmetry that probes the AN zone of the first BZ, the B_{2g} symmetry probes the N zone of the first BZ. And the A_{1g} symmetry probes the whole Brillouin zone. Here, we do not consider the A_{2g} symmetry, $\gamma^{A_{2g}} = 0$. In the following, we only focus on the B_{1g} and B_{2g} symmetry. The specific case of A_{1g} symmetry has already been studied in the framework of a charge order and superconducting coexisting state⁷¹. In both the B_{1g} and the B_{2g} symmetries, the Coulombian screening can be neglected⁷⁰. In the B_{1g} and B_{2g} symmetries, the bare Raman susceptibility write^{46,70}:

$$\chi_\lambda(\omega, \mathbf{q} = 0) = -\frac{T}{2} \sum_{\epsilon, \mathbf{k}} \text{Tr} \left[\bar{\gamma}^\lambda(\mathbf{k}) \hat{G}(\omega + \epsilon, \mathbf{k}) \bar{\gamma}^\lambda(\mathbf{k}) \hat{G}(\epsilon, \mathbf{k}) \right], \quad (11)$$

where $\bar{\gamma}^\lambda(\mathbf{k}) = \gamma^\lambda(\mathbf{k}) \bar{\tau}_3$ with τ_3 is the Pauli matrix evolving in the particle-hole space in the λ symmetry (with $\lambda = B_{1g}$ or B_{2g}).

III. RESULTS

We perform a study at optimal doping $p = 0.16$ and in the underdoped regime $p = 0.1$ in Hg-1201. At both $p = 0.1$ and $p = 0.16$, the SC critical temperature T_c is lower than the T^* , $T_c < T^*$. We consider that in the SC state $T < T_c$, the SC and RES coexist while above T_c ($T_c < T < T^*$) only the RES remains. The RES disappears at T^* .

At $p = 0.1$, we choose $\Delta_{RES}^0 = 0.09\text{eV}$ and $\Delta_{SC}^0 = 0\text{eV}$ in the RES state while $\Delta_{RES}^0 = 0.06\text{eV}$ and $C^0 = 0.06\text{eV}$ in the SC state. The order magnitude of the RES and SC order parameter on the Fermi surface is presented in Fig. 4 a) and b). The SC order parameter develops in the N region and decreases in the AN zone while the RES order parameter vanishes in the N region and increases in the AN region. At the zone edges, the SC gap represents 30% of the whole gap magnitude while the RES is at 70%.

At optimal doping ($p = 0.16$), we choose $\Delta_{RES}^0 = 0.065\text{eV}$ and $\Delta_{SC}^0 = 0\text{eV}$ in the RES state while $\Delta_{RES}^0 =$

0.01eV and $C^0 = 0.042eV$ in the SC state as presented on Fig. 5. The SC order parameter develops on the whole Fermi surface while the RES order parameter only exists in the AN zone. At the zone edges, the SC gap represents 95% of the whole gap magnitude while the RES is at 5%. The SC order parameter exhibits a d -wave aspect at optimal doping while this aspect is weakened in the underdoped regime. The RES gap dependence is different than a pure d -wave dependence as observed by ARPES in Bi-2212⁶⁶ and Hg-1201⁶⁷.

From a technical point of view, the calculation of the bare polarization bubbles is done as follow. The summation over the internal impulsion is done in a 400x400 grid in the first BZ after doing the analytical integration over the internal Matsubara frequencies at $T = 0K$. Note that we neglected the temperature dependence of the order parameters. We have done the analytical continuation on the external Matsubara frequency replacing $i\omega$ by $\omega + i\eta$ where η is a small damping parameter taken here to $\eta = 3meV$. This small parameter can be understood as residual scattering caused by the impurities. The susceptibilities are in the unit of states per eV per CuO₂ formula unit and should be multiplied $2\mu_B^2$ to compare to neutron-scattering data (μ_B is the Bohr magneton).

A. The density of states.

The electronic density of states (DOS), $\rho(\omega) = \frac{-2}{\pi} \sum_{\mathbf{k}} [\text{Im}(\lim_{\eta \rightarrow 0} G^{11}(\omega + i\eta, \mathbf{k}))]$ in the normal metal, RES and SC phases are plotted in Fig. 4 for hole doping $p = 0.1$ and Fig. 5 for $p = 0.16$. Both SC and RES open a symmetric gap at the Fermi level ($\omega = 0$). At $p = 0.1$, the magnitude of the gap is 54 meV in the SC phase and 75 meV in the RES phase. At $p = 0.16$, the magnitude of the gap is 39 meV in the SC phase and 59 meV in the RES phase. The amplitude of the gap in the RES and the SC state are in good agreement with experimental gaps deduced from Raman scattering^{47,48}. The low energy behavior of the DOS differs a little between the RES and the SC state. The coherent peak seen in the SC state is weakened in the RES state as observed in cuprate compounds⁷². Note that the Van Hove singularity is well defined by a peak at negative energy. The form of the DOS at low energy (close to $\omega = 0eV$) is typical of the d -wave momentum dependence of the SC gap⁷² but does not give more information about the nature of the order parameter. In order to observe specific signature of both RES and SC state, we need probes that are sensible to the coherence between the quasiparticles such as Raman scattering and INS.

B. The Raman susceptibility

We calculate the Raman response in the B_{1g} and the B_{2g} symmetry in the SC state at $p = 0.1$ and $p = 0.16$ (see Fig. 6)^{46,70}. Our approximation is able to reproduce

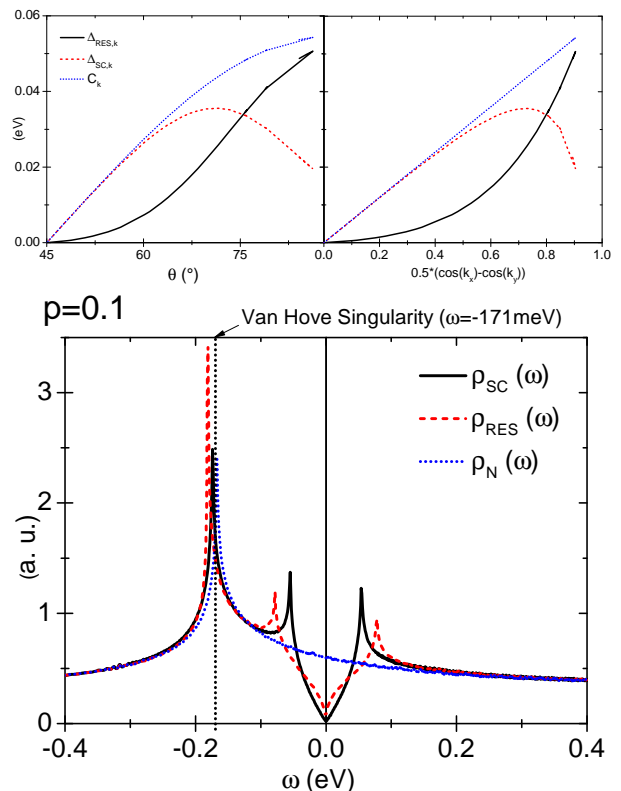


FIG. 4. Dependence of the RES (solid line), SU(2) envelop (dotted line) and SC gap (dashed line) on the FS as a function of left panel) the θ angle and right panel) the d -wave factor at $p = 0.1$. The SC gap exhibits a d -wave behavior close to the nodal zone and its intensity decreases in the AN zone. Bottom panel) Density of states in the Normal metal $\rho^N(\omega)$ (dotted lines), the RES $\rho^{RES}(\omega)$ (solid lines) and the SC state $\rho^{SC}(\omega)$ (dashed line) as a function of energy ω for $p = 0.1$. The SC and RES order parameters open a symmetric gap centered around the Fermi level $\omega = 0eV$. The d -wave symmetry leads to the typical form of the density of state at low energy. The Van-Hove singularity arises in the metallic spectrum at $\omega = -171meV$ for $p = 0.1$. The magnitude of the gap is 54 meV in the SC phase and 75 meV in the RES phase. Note that the amplitude of the gaps are qualitatively in accordance with the experimental data.

the decreasing of the frequency resonance in the B_{1g} symmetry with hole doping, (see Fig. 6) from $\omega_{sc} = 101meV$ at $p = 0.1$ until $\omega_{sc} = 77meV$ at $p = 0.16$. Moreover, the intensity of the B_{1g} Raman resonance is lower at low doping ($p=0.1$) than close to optimal doping ($p=0.16$). Both features are in good agreement with experimental Raman scattering in Hg-1201 compound^{47,48}.

In the B_{1g} , the superconducting coherence peak occurs at the energy $2\sqrt{\Delta_{RES}^2(\mathbf{k}_{ZE}) + \Delta_{SC}^2(\mathbf{k}_{ZE})}$ where \mathbf{k}_{ZE} is the point of the FS localized at the zone edge (see Fig. 2). The frequency of the superconducting coherent peak depends on the magnitude of both the SC and RES order parameters at the zone edge. Consequently, this frequency is larger than twice the magnitude of the SC

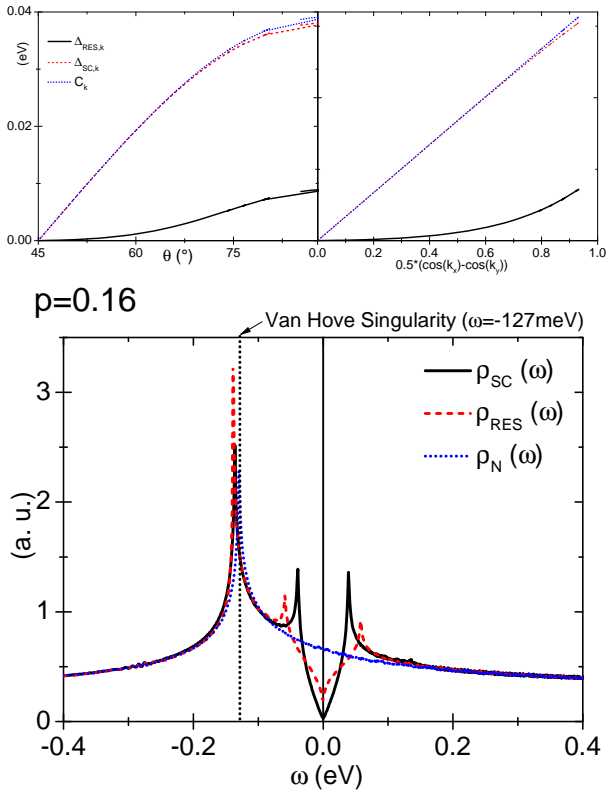


FIG. 5. Dependence of the RES (solid line), SU(2) envelop (dotted line) and SC gap (dashed line) on the FS as a function of left panel) the θ angle and right panel) the d -wave factor at $p = 0.1$. The SC order parameter as d -wave behavior in the whole Brillouin zone. Bottom panel) Density of states in the Normal metal $\rho^N(\omega)$ (dotted lines), the RES $\rho^{RES}(\omega)$ (solid lines) and the SC state $\rho^{SC}(\omega)$ (dashed line) as a function of energy ω for $p = 0.16$. The SC and RES order parameters open a symmetric gap centered around the Fermi level $\omega = 0$ eV. The d -wave symmetry leads to the typical form of the density of state at low energy. The Van-Hove singularity arises in the metallic spectrum at $\omega = -292$ meV for $p = 0.16$. The magnitude of the gap is 39 meV in the SC phase and 59 meV in the RES phase. Note that the amplitudes of the gaps are qualitatively in accordance with the experimental data.

order parameter and does not scale with T_c . However, the intensity of the SC coherent peak only depends on the magnitude of the SC order parameter at the zone edge. In step with the SC gap dependence discussed in section II A and shown in Figs. 4 and 5, the intensity of the SC coherent peak in the B_{1g} symmetry increases with the hole doping.

In the B_{2g} channel, we see the emergence of a peak at low frequency^{47,48}. The d -wave symmetry of the gap implies a small intensity of the SC coherent peak.

C. The bare spin susceptibility

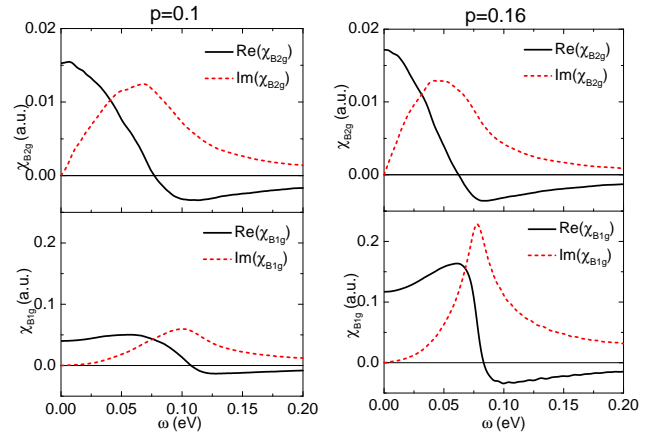


FIG. 6. The Raman susceptibility in the B_{1g} and the B_{2g} symmetry at a) $p = 0.1$ in the RES state, b) and b) $p = 0.16$. The calculated responses are in promising agreement with the experimental data. In the B_{2g} channel, the intensity does not vary with doping but the frequency resonance increases at low doping. In the B_{1g} channel, the frequency resonance increases at low doping but the intensity fall down as observed experimentally.

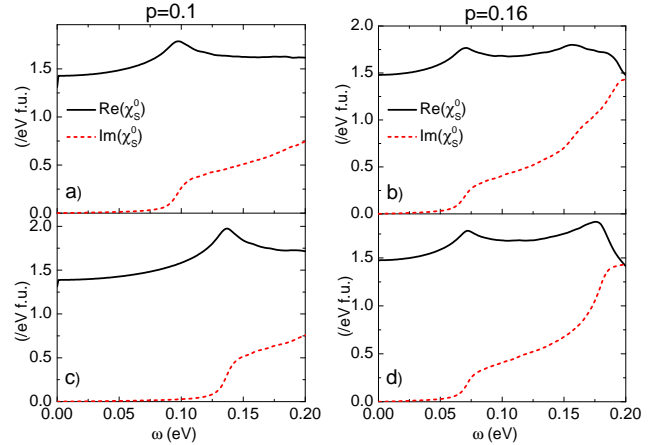


FIG. 7. The real and imaginary parts of the bare polarization bubble at $\mathbf{Q} = (\pi, \pi)$ for a) $p = 0.1$ in the RES state, b) $p = 0.16$ in the RES state c) $p = 0.1$ in the SC state, d) $p = 0.16$ in the SC state. The amplitude of the order parameters are the same as in Figs. 4 and 5. We observe a gap opening in both SC state and RES.

The real and imaginary parts of the bare polarization bubble in the RES and SC phases at hole doping $p = 0.1$ and $p = 0.16$ are presented in Fig. 7 as a function of ω at $\mathbf{Q} = (\pi, \pi)$. In the RES, (Figs. 7 a) and b)), a gap opens in the imaginary part of χ_s^0 very similarly than the quasiparticle gap opening in the SC state (Figs. 7 c) and d)). In the RES, the threshold in the Imaginary part and the logarithmic divergence in the real part occur at energies close to $2\Delta_{RES}(\mathbf{k}_{HS})$. The energy of the threshold move from 94 meV at $p = 0.1$ until 64 meV at $p = 0.16$ in the RES. On the other hand, the threshold is defined at the energy $2\sqrt{\Delta_{RES}^2(\mathbf{k}_{HS}) + \Delta_{SC}^2(\mathbf{k}_{HS})}$

in the SC phase. The energy of the threshold moves from 129 meV at $p = 0.1$ down to 66 meV at $p = 0.16$ in the SC. The bare spin susceptibilities in the SC and RES states are very similar because the gap mechanism is nearly the same close to the FS. This feature is emphasized by the fact that close to the FS, we can apply the identity $\xi_{\mathbf{k}-2\mathbf{p}_F(\mathbf{k})} = -\xi_{\mathbf{k}}$ and the bare spin susceptibility in the RES becomes the same than the SC one.

D. The RPA spin susceptibility

The amplitude of the imaginary part of the RPA susceptibility for the RES and SC phases are presented in Figs. 8 and 9 for $p = 0.1$ and $p = 0.16$ respectively, as a function of ω in the diagonal direction $q_y = q_x$ and q_x from $-\pi/2a$ to $3\pi/2a$ (with a that the unit cell parameter set to unity).

At $p = 0.16$, the magnitude of the super-exchange interaction $J_0 = 151 \text{ meV}$ is adjusted to set the resonance at \mathbf{Q} at 60 meV while at $p = 0.1$, we put $J_0 = 169 \text{ meV}$ to ensure a resonance at 50 meV . In both RES and SC state, we observe a resonance at \mathbf{Q} . The intensity as well as the form of the resonance does not vary a lot between the two states at both doping. (Figs. 8 c) and 9 c). The shape of the energy fluctuations close to \mathbf{Q} does not qualitatively change between the SC and RES at $p = 0.1$ (Figs. 8 a) and b)) while this change is strong at optimal doping (Figs. 9 a) and b)). The change in the form is a clear effect of the loss of coherence between the patches away from the \mathbf{Q} vector in the RES.

At $p = 0.1$, the RES order parameter is dominant in both SC and RES state resulting on a Y-shape in both cases. At optimal doping, the SC order parameter dominates in the SC states leading to the X-shape. The loss of coherent terms in the RES erases the X-shape observed in the SC state.

IV. DISCUSSION

We discuss below the three main findings of our theory, compared to other approaches proposed so far.

First, as shown in Figs. 8 and 9 the model gives a good agreement for the frequency resonance and the intensity of the resonance observed at \mathbf{Q} in Hg-1201. The frequency resonance is determined by the values of the RES and SC order parameters as well as the value of the super-exchange J_0 . The values of the RES and SC order parameter have been determined to reproduce the Raman coherent peak in the B_{1g} and B_{2g} symmetry. The value of $J_0 = 169 \text{ meV}$ at $p = 0.1$ and $J_0 = 151 \text{ meV}$ at $p = 0.16$ is in the right range of values for cuprate compounds. Moreover, the decrease of the magnitude with doping is consistent with the decrease of the two-magnon peak in Raman data^{47,48}. The frequency and intensity of the resonance is the same in both the SC and the RES in the underdoped regime and optimal doping²⁶⁻²⁸. At

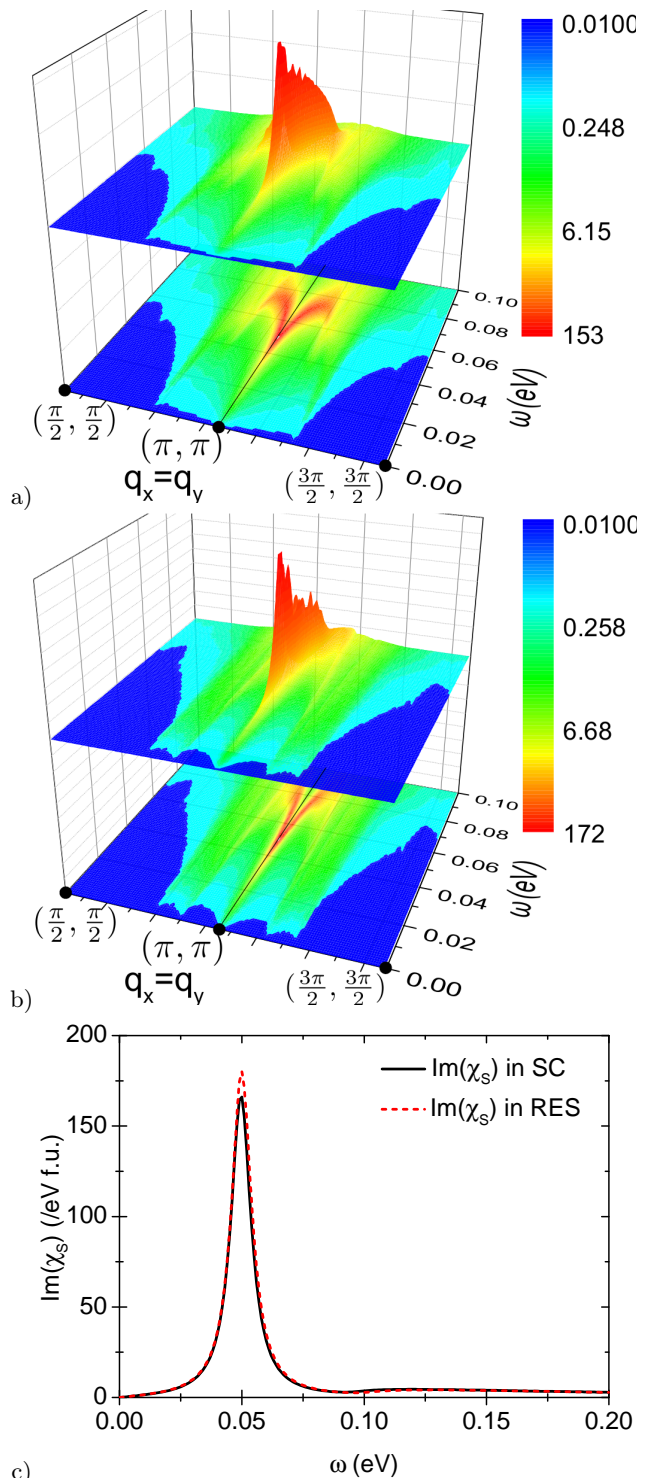


FIG. 8. Amplitude of the Imaginary part of the spin susceptibility χ_S as a function of ω , for $q_y = q_x$ and q_x from $-\pi/2a$ to $3\pi/2a$ at $p = 0.1$ for $J_0 = 169 \text{ meV}$ and $V = 100$ in a) the SC state and b) the RES. The solid line is set at $q = (\pi/a, \pi/a)$. c) Cut at $\mathbf{Q} = (\pi, \pi)$ of the imaginary part of χ_S in the RES (dashed line) and SC (solid line) state.

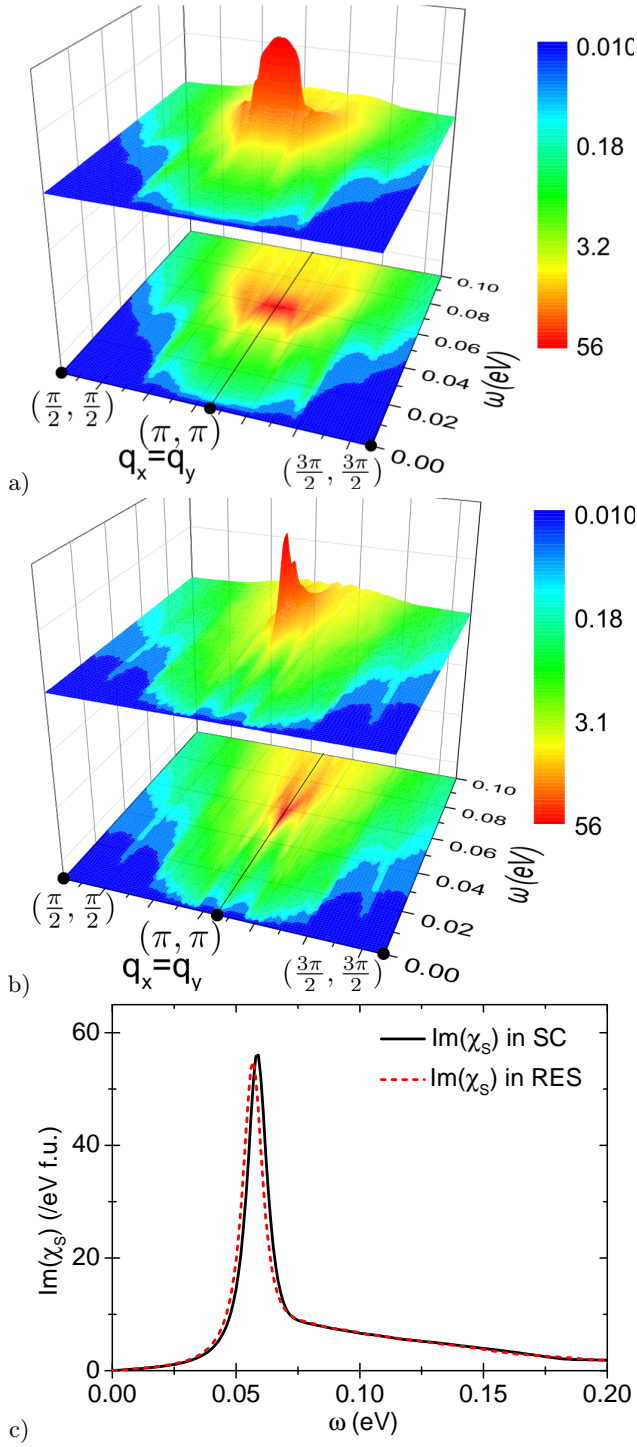


FIG. 9. Amplitude of the Imaginary part of the spin susceptibility χ_S as a function of ω , for $q_y = q_x$ and q_x from $-\pi/2a$ to $3\pi/2a$ at $p = 0.16$ for $J_0 = 151 \text{ meV}$ and $V = 100$ in a) the SC state and b) the RES. The solid line is set at $q = (\pi/a, \pi/a)$. c) Cut at $\mathbf{Q} = (\pi, \pi)$ of the imaginary part of χ_S in the RES (dashed line) and SC (solid line) state.

optimal doping, the same intensity observed in both RES and SC state is in agreement with the absence of any signature on the intensity of the resonance at T_c ^{26–28}. The same intensity in both the RES and SC state is a by-product of our model where we did not adjust the damping that could be higher in a non-homogeneous state as RES. Indeed, our model produces naturally intrinsic inhomogeneities due to the proliferation of local objects. This aspect will be studied in future publications.

Second, our model reproduces in a promising agreement the fluctuation spectrum around \mathbf{Q} in both the SC and RES state. The disappearance of the low energy fluctuation spectrum in the SC state when we pass to the RES (and then the transformation from the X-shape to the Y-shape) can be explained by the loss of the coherence terms in the RES away from the vector \mathbf{Q} . The enhancement of the coherence close to the \mathbf{Q} vector leads to the increasing of the value of the spin susceptibility at \mathbf{Q} in the RES and the emergence of the Y shape in the energy fluctuation spectrum. In our model, we have modeled this loss of coherence by a function $f(\mathbf{q})$ which vanishes away from \mathbf{Q} . The effect of the width of the function $f(\mathbf{q})$ on the spin susceptibility is studied in the Appendix B.

A simple explanation for the emergence of spectral weight at \mathbf{Q} in the pseudo gap phase can be given as follows. Since their origin lies in the SU(2) fluctuations, the RES patches are acting on a small part of the BZ, and are gapping out the anti-nodal region of the Fermi surface, close to the hot spots. Fluctuations associated with the SU(2) scenario are thus restricted to these regions. The typical wave vectors connecting these regions to one another are $\mathbf{q} = \mathbf{Q}$ and $\mathbf{q} = \mathbf{0}$, but due to the presence of the d -wave phase factor, the positive sign necessary for forming bound state (as opposed to anti-bound) selects the wave vector \mathbf{Q} . Hence the two main ingredients for the emergence of spectral weight at \mathbf{Q} and the presence of the factor $f(\mathbf{q})$ in Eqn.(9) are the localization of the RES around the hot spots (which selects the mode modulation vectors $\mathbf{q} = \mathbf{0}$ and $\mathbf{q} = \mathbf{Q}$) in the anti-nodal region and retaining a certain coherence with d -wave form factor (which finally selects the modulation vector around $\mathbf{q} = \mathbf{Q}$). In order to test this idea, we show in Appendix C the same calculation for a SC state with the SC gap formation restricted to a small region around the hot spots. We see in Fig. 12 that it gives some additional spectral weight around $\mathbf{q} = \mathbf{Q}$ as desired. For a SC state, the form of the additional spectral weight is more like a spot rather than the “Y”-shape. The elongation of the tail of the “Y” at \mathbf{Q} is a consequence of the “nesting” feature $\mathbf{k} \rightarrow \mathbf{k} - 2\mathbf{p}_F$ when the energy is lowered.

Lastly, the dependence in doping of the fluctuation spectrum can be explained by the nature of the RES. The proliferation of excitonic patches occurs at zero temperature at low doping while it occurs at much higher temperature close to optimal doping (see Fig. 1). This difference implies that RES order is strong at low doping and coexist with SC order parameter while it weakens at op-

timal doping consistently with Raman experiments^{47,48}. Consequently, the RES state drives the physics close to AF critical vector at low doping explaining the Y-shape of energy fluctuation spectrum in both SC and RES. At optimal doping, the RES weakens in the AN zone and the physics is dominated by SC order parameter which implies the appearance of the X-shape.

A possible extension of this work should be the calculation of the RES response in bilayered systems. In such systems, the interlayer coupling creates bonding and anti-bonding states and gives rise to even and odd spin susceptibilities. Leaving aside the stability of the RES in such bilayer compounds, we expect the even and odd susceptibilities to behave similarly than in the monolayer compound. However, the exact vector where the resonance occurs could change because of the mismatch between the bonding and anti-bonding Fermi surfaces. The effect of exotic structure like CuO chains in YBCO compounds on the spin dynamics is still unclear. The CuO chains could stabilize nematic orders⁷³ which could reciprocally affect of spin susceptibility and produce incommensurability. This nematic order could be strong in the SU(2) scenario⁴⁹. We let the detailed calculations for forthcoming publications.

V. CONCLUSION

We proposed a description of the energy spectrum of the dynamic spin susceptibility, observed by INS in recent experiments on the cuprate compounds Hg-1201, for both the SC and the PG states. This explanation is based on a new concept for the PG phase which shows the emergence of particle-hole pairs, forming excitonic droplets, or patches with multiple modulation wave vectors $2\mathbf{p}_F$. The RES state behaves “almost” like a d -wave SC, but gaps out the anti-nodal region of the first BZ, leading to the formation of Fermi “arcs”⁶⁴. In the PG regime, this restriction provokes a loss of coherence terms except at some peculiar wave vectors commensurate with the lattice, like the AF vector \mathbf{Q} . This description of the PG phase is able to reproduce the main features of the Raman scattering in Hg-1201, and is a promising candidate for PG state of superconducting cuprates.

ACKNOWLEDGMENTS

The authors acknowledge Y. Sidis, P. Bourges, S. Hayden, M. Greven and T. Kloss for fruitful discussions. This work was supported by LabEx PALM (ANR-10-LABX-0039- PALM), of the ANR project UNESCO ANR-14-CE05-0007, the ERC, under grant agreement AdG-694651-CHAMPAGNE, the Aspen Center for Physics, as well as the Grant No. Ph743-12 of the COFECUB which enabled frequent visits to the IIP, Natal. X.M. also acknowledge the support of CAPES and funding from the IIP.

Appendix A: Feynman Diagram in the spin susceptibility

We consider the spin susceptibility originating the t-J model^{31,62} which writes:

$$\chi_S(\omega, \mathbf{q}) = \frac{\chi_S^0(\omega, \mathbf{q})}{1 + J(\mathbf{q})\chi_S^0(\omega, \mathbf{q})} \quad (\text{A1})$$

with $J(\mathbf{q}) = J_0(\cos(q_x a_0) + \cos(q_y a_0))$. In the equation (6), χ_S^0 is the bare polarization bubble constructed from the Green’s function and $J(\mathbf{q})$ is super-exchange interaction. Note that momentum dependence of the super-exchange term $J(\mathbf{q})$ originates the exchange between near neighbor Copper site. The bare polarization can be evaluated by the formula^{33,69}:

$$\chi_S^0(\omega, \mathbf{q}) = -\frac{T}{2} \sum_{\epsilon, \mathbf{k}} \text{Tr} \left[\hat{G}(\omega + \epsilon, \mathbf{k} + \mathbf{q}) \hat{G}(\epsilon, \mathbf{k}) \right] \quad (\text{A2})$$

where $\epsilon(\omega)$ is the fermionic (bosonic) Matsubara frequency, $\mathbf{k}(\mathbf{q})$ is the impulsion, T the temperature and Tr means Trace of the Green function matrix \hat{G} . The relation (A2) describes the whole polarization of the system that is the sum of the polarizations Π :

$$\chi_S^0 = \frac{1}{8} \left(\sum_{i,j} \Pi^{ij} \right) \quad (\text{A3})$$

where Π^{ij} are the polarizations described by the diagrams of the Fig.10 with $\Pi^{ij} = -T \sum_{\epsilon, \mathbf{k}} [G^{ij}(\omega + \epsilon, \mathbf{k} + \mathbf{q}) G^{ij}(\epsilon, \mathbf{k})]$ with $\Pi^{ij} = \Pi^{ji}$ for $j \neq i$. $\Pi^{11(44)}$ (diagram (a) (and (d)) of Fig.10) is the response of the electrons (holes) with momentum \mathbf{k} while $\Pi^{22(33)}$ (diagram (b) (and (c)) of Fig.10) is the response of the electrons (holes) with momentum $\mathbf{k} + 2\mathbf{p}_F(\mathbf{k})$. The polarization $\Pi^{41(32)}$ (diagram (e) (and (f)) of Fig.10) is the response of the Cooper pairs while $\Pi^{31(42)}$ (diagram (g) (and (h)) of Fig.10) is the response of the particle-hole pairs. The polarization $\Pi^{21(43)}$ (diagram (i) (and (j)) of Fig.10) is the mixed SC-RES response. Note that the superconducting coherent factors comes from the terms $\Pi_{SC}^{41(32)}$.

As shown in the diagram (g) to (j) of Fig.10, the outgoing external vector depends on the difference $\bar{\delta}_{2\mathbf{p}_F} = 2\mathbf{p}_F(\mathbf{k} + \mathbf{q}) - 2\mathbf{p}_F(\mathbf{k})$. In order to these diagrams to contribute to the global polarization ($\Pi^{21(31,42,43)} \neq 0$), this difference must vanish, $\bar{\delta}_{2\mathbf{p}_F} = \mathbf{0}$. Obviously, this difference vanishes for $\mathbf{q} = \mathbf{0}$. This difference also vanishes for $\mathbf{q} = \mathbf{Q}$. The RES polarization contributes around $\mathbf{q} \approx \mathbf{0}$ and $\mathbf{q} \approx \mathbf{Q}$ but will vanish if \mathbf{q} is far from $\mathbf{0}$ or \mathbf{Q} . To take modelize this effect, we introduce a momentum dependent function in the relation (A3) which transforms itself as :

$$\chi_S^0 = \frac{1}{8} \left(\Pi^{11} + \Pi^{22} + \Pi^{33} + \Pi^{44} + 2(\Pi^{32} + \Pi^{41}) + 2f(\mathbf{q})(\Pi_{RES}^{21} + \Pi_{RES}^{31} + \Pi_{RES}^{42} + \Pi_{RES}^{43}) \right) \quad (\text{A4})$$

where $f(\mathbf{q})$ acts on the RES and SC-RES mixed polarizations. The function $f(\mathbf{q})$ has the form :

$$f(\mathbf{q}) = \frac{1}{1 + V(\sin^2(q_x a) + \sin^2(q_y a))} \quad (\text{A5})$$

which is a Lorentzian centered in $\mathbf{q} = (0, 0)$ and $\mathbf{q} = \mathbf{Q} = (\pi, \pi)$ whose width can be tuned by the parameter V . If V tends toward zero, the function $f(\mathbf{q})$ uniformly tends to unity. If V tends toward infinity, the function $f(\mathbf{q})$ is a dirac distribution centered in $(0, 0)$ and (π, π) . The effect of the function f on the spin susceptibility is detailed in the Appendix B.

Appendix B: Effect of the f function on the spin susceptibility χ_S around \mathbf{Q}

In this section we present the effect of the width of the function f on the spin susceptibility χ_S . The function f is a Lorentzian whose width can be tune by the value of

the parameter V (see formula A5). If V vanishes then f is uniformly unity, $f = 1$. If V tends toward infinity then f becomes a Dirac function centered in \mathbf{Q} . In the Fig. 11, we present the spin susceptibility χ_S as a function of the parameter V . We observe that the for $V = 0$ (Fig. 11 c)), the energy fluctuation in the RES looks like the one in the pure SC state³³ with the two branches from either side of the momentum \mathbf{Q} but with a particle-hole continuum at \mathbf{Q} . When the parameter V increases (Fig. 11 a) and b)), the two branches are completely lowered and only the resonance at \mathbf{Q} remains.

Appendix C: Effect of the SC order parameter momentum dependence on the spin susceptibility

In this section, we present the effect of the momentum dependence of the SC order parameter on the form of the spin susceptibility. If we consider a SC gap centered only on the hot-spot (see Fig. 12 a)), the spin susceptibility is maximal around the vector (π, π) only and the X shape disappears, as shown in Fig. 12 b).

* xavier.montiel@rhul.ac.uk

† catherine.pepin@cea.fr

¹ H. Alloul, T. Ohno, and P. Mendels, *Phys. Rev. Lett.* **63**, 1700 (1989).

² W. W. Warren, R. E. Walstedt, G. F. Brennert, R. J. Cava, R. Tycko, R. F. Bell, and G. Dabbagh, *Phys. Rev. Lett.* **62**, 1193 (1989).

³ J. Tallon and J. Loram, *Physica C* **349**, 53 (2001).

⁴ J. M. Tranquada, G. Shirane, B. Keimer, S. Shamoto, and M. Sato, *Phys. Rev. B* **40**, 4503 (1989).

⁵ D. Reznik, P. Bourges, H. F. Fong, L. P. Regnault, J. Bossy, C. Vettier, D. L. Milius, I. A. Aksay, and B. Keimer, *Phys. Rev. B* **53**, R14741 (1996).

⁶ J. Rossat-Mignod, L. Regnault, C. Vettier, P. Bourges, P. Burllet, J. Bossy, J. Henry, and G. Lapertot, *Physica C* **185-189, Part 1**, 86 (1991).

⁷ H. A. Mook, M. Yethiraj, G. Aeppli, T. E. Mason, and T. Armstrong, *Phys. Rev. Lett.* **70**, 3490 (1993).

⁸ H. F. Fong, B. Keimer, P. W. Anderson, D. Reznik, F. Doğan, and I. A. Aksay, *Phys. Rev. Lett.* **75**, 316 (1995).

⁹ P. Bourges, Y. Sidis, H. F. Fong, L. P. Regnault, J. Bossy, A. Ivanov, and B. Keimer, *Science* **288**, 1234 (2000).

¹⁰ S. Pailhès, Y. Sidis, P. Bourges, V. Hinkov, A. Ivanov, C. Ulrich, L. P. Regnault, and B. Keimer, *Phys. Rev. Lett.* **93**, 167001 (2004).

¹¹ V. Hinkov, S. Pailhès, P. Bourges, Y. Sidis, A. Ivanov, A. Kulakov, C. T. Lin, D. P. Chen, C. Bernhard, and B. Keimer, *Nature* **430**, 650 (2004).

¹² P. Dai, H. A. Mook, S. M. Hayden, G. Aeppli, T. G. Perring, R. D. Hunt, and F. Doğan, *Science* **284**, 1344 (1999).

¹³ P. Dai, M. Yethiraj, H. A. Mook, T. B. Lindemer, and F. Doğan, *Phys. Rev. Lett.* **77**, 5425 (1996).

¹⁴ H. F. Fong, B. Keimer, D. L. Milius, and I. A. Aksay, *Phys. Rev. Lett.* **78**, 713 (1997).

¹⁵ H. F. Fong, P. Bourges, Y. Sidis, L. P. Regnault, J. Bossy, A. Ivanov, D. L. Milius, I. A. Aksay, and B. Keimer, *Phys. Rev. B* **61**, 14773 (2000).

¹⁶ G. Aeppli, S. M. Hayden, H. A. Mook, Z. Fisk, S.-W. Cheong, D. Rytz, J. P. Remeika, G. P. Espinosa, and A. S. Cooper, *Phys. Rev. Lett.* **62**, 2052 (1989).

¹⁷ P. Bourges, B. Keimer, S. Pailhès, L. Regnault, Y. Sidis, and C. Ulrich, *Physica C* **424**, 45 (2005).

¹⁸ H. He, Y. Sidis, P. Bourges, G. D. Gu, A. Ivanov, N. Koshizuka, B. Liang, C. T. Lin, L. P. Regnault, E. Schoenherr, and B. Keimer, *Phys. Rev. Lett.* **86**, 1610 (2001).

¹⁹ T. E. Mason, A. Schröder, G. Aeppli, H. A. Mook, and S. M. Hayden, *Phys. Rev. Lett.* **77**, 1604 (1996).

²⁰ T. E. Mason, G. Aeppli, S. M. Hayden, A. P. Ramirez, and H. A. Mook, *Phys. Rev. Lett.* **71**, 919 (1993).

²¹ M. K. Chan, C. J. Dorow, L. Mangin-Thro, Y. Tang, Y. Ge, M. J. Veit, G. Yu, X. Zhao, A. D. Christianson, J. T. Park, Y. Sidis, P. Steffens, D. L. Abernathy, P. Bourges, and M. Greven, *Nat. Commun.* **7**, 10819 (2016).

²² C. Stock, W. J. L. Buyers, R. Liang, D. Peets, Z. Tun, D. Bonn, W. N. Hardy, and R. J. Birgeneau, *Phys. Rev. B* **69**, 014502 (2004).

²³ C. Stock, W. J. L. Buyers, R. A. Cowley, P. S. Clegg, R. Coldea, C. D. Frost, R. Liang, D. Peets, D. Bonn, W. N. Hardy, and R. J. Birgeneau, *Phys. Rev. B* **71**, 024522 (2005).

²⁴ S. M. Hayden, H. A. Mook, P. Dai, T. G. Perring, and F. Dogan, *Nature* **429**, 531 (2004).

²⁵ J. M. Tranquada, H. Woo, T. G. Perring, H. Goka, G. D. Gu, G. Xu, M. Fujita, and K. Yamada, *Nature* **429**, 534 (2004).

²⁶ B. Vignolle, S. M. Hayden, D. F. McMorrow, H. M. Ronnow, B. Lake, C. D. Frost, and T. G. Perring, *Nat. Phys.* **3**, 163 (2007).

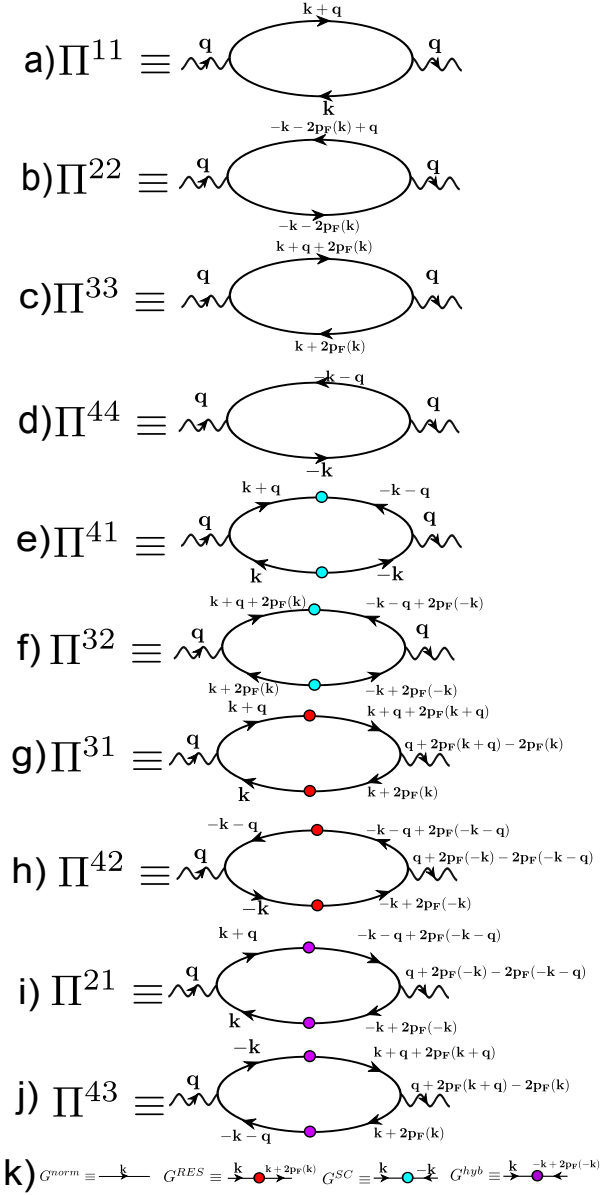


FIG. 10. Polarizations Π^{ij} that contribute to the bare polarization χ_0 (see equation (A3)). In a) to d) are the diagrammatic representation of the polarization with normal contribution. In e) an f) are presented the contribution of superconducting state. In g) and h) are presented the contribution of the RES. In i) and j) are shown the mixed SC-RES contribution. The contribution of the RES and SC-RES mixed polarization (diagrams from g) to j)) only exist for q close to $(0,0)$ and (π,π) . In k) are presented the diagrammatic representation of the Green function.

²⁷ V. Hinkov, P. Bourges, Y. Pailhès, S. and Sidis, A. Ivanov, C. D. Frost, T. G. Perring, C. T. Lin, D. P. Chen, and B. Keimer, *Nat. Phys.* **3**, 780 (2007).

²⁸ J. M. Tranquada, G. Xu, T. G. Perring, M. Hucker, G. D. Gu, B. Fauque, and L. P. Regnault, *Nat. Phys.* **5**, 642 (2009).

²⁹ F. Onufrieva and P. Pfeuty, *Phys. Rev. B* **61**, 799 (2000).

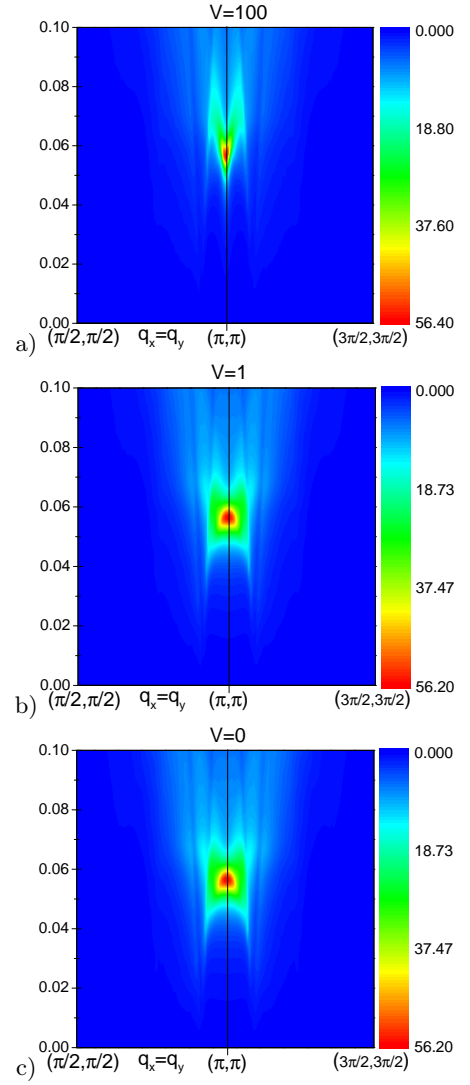


FIG. 11. Amplitude of the Imaginary part of the spin susceptibility χ_S as a function of ω , for $q_y = q_x$ and q_x from $-\pi/2a$ to $3\pi/2a$ at $p = 0.16$ for $J_0 = 0.2225$ as a function of the parameter V . In a) $V=100$, in b) $V=1$ and in c) $V=0$. The solid line is set at $q = (\pi/a, \pi/a)$. The susceptibility χ_S is calculated in the RES state at $p = 0.16$ and the order parameter magnitude are $\Delta_{SC}^0 = 0meV$ and $\Delta_{RES}^0 = 100meV$. The value of V affects the width of the function f . For $V = 0$, we clearly observe two branches from either side of momentum \mathbf{Q} which are cut with higher value of V .

³⁰ F. Onufrieva and P. Pfeuty, *Phys. Rev. B* **65**, 054515 (2002).

³¹ J. Brinckmann and P. A. Lee, *Phys. Rev. Lett.* **82**, 2915 (1999).

³² E. Demler and S.-C. Zhang, *Phys. Rev. Lett.* **75**, 4126 (1995).

³³ M. R. Norman, *Phys. Rev. B* **75**, 184514 (2007).

³⁴ O. Tchernyshyov, M. R. Norman, and A. V. Chubukov, *Phys. Rev. B* **63**, 144507 (2001).

³⁵ G. Stemmam, C. Pépin, and M. Lavagna, *Phys. Rev. B* **50**, 4075 (1994).

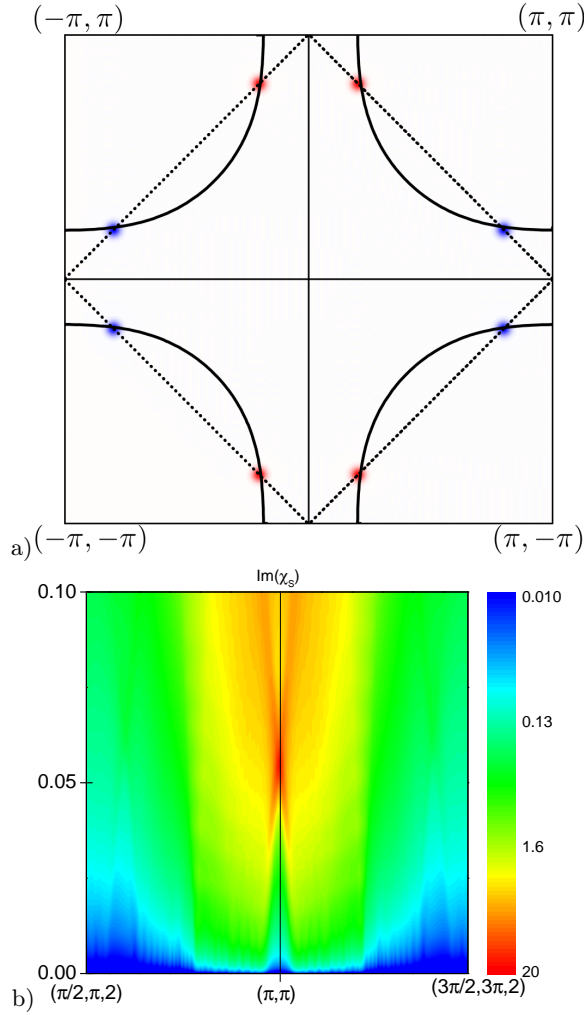


FIG. 12. a) Amplitude of the superconducting gap in the first Brillouin zone. The superconducting gap is centered on the hot-spots. b) Amplitude of the Imaginary part of the spin susceptibility χ_S as a function of ω , for $q_y = q_x$ and q_x from $-\pi/2a$ to $3\pi/2a$ at $p = 0.16$ for $J_0 = 0.2225$. The amplitude is centered in the (π, π) and the X-shape disappears.

³⁶ D. Manske, I. Eremin, and K. H. Bennemann, *Phys. Rev. B* **63**, 054517 (2001).
³⁷ I. Eremin, D. K. Morr, A. V. Chubukov, K. Bennemann, and M. R. Norman, *Phys. Rev. Lett.* **94**, 147001 (2005).
³⁸ M. Eschrig and M. R. Norman, *Phys. Rev. Lett.* **85**, 3261 (2000).
³⁹ M. Eschrig and M. R. Norman, *Phys. Rev. Lett.* **89**, 277005 (2002).
⁴⁰ M. Eschrig and M. R. Norman, *Phys. Rev. B* **67**, 144503 (2003).
⁴¹ M. Eschrig, *Adv. Phys.* **55**, 47 (2006).
⁴² E. Demler, W. Hanke, and S.-C. Zhang, *Rev. Mod. Phys.* **76**, 909 (2004).
⁴³ A. V. Chubukov, B. Jankó, and O. Tchernyshyov, *Phys. Rev. B* **63**, 180507 (2001).
⁴⁴ A. Abanov, A. V. Chubukov, M. Eschrig, M. R. Norman, and J. Schmalian, *Phys. Rev. Lett.* **89**, 177002 (2002).
⁴⁵ F. Onufrieva, *Phys. Rev. B* **95**, 125110 (2017).

⁴⁶ T. P. Devereaux and R. Hackl, *Rev. Mod. Phys.* **79**, 175 (2007).
⁴⁷ Y. Li, M. Le Tacon, M. Bakr, D. Terrade, D. Manske, R. Hackl, L. Ji, M. K. Chan, N. Barišić, X. Zhao, M. Greven, and B. Keimer, *Phys. Rev. Lett.* **108**, 227003 (2012).
⁴⁸ Y. Li, M. Le Tacon, Y. Matiks, A. V. Boris, T. Loew, C. T. Lin, L. Chen, M. K. Chan, C. Dorow, L. Ji, N. Barišić, X. Zhao, M. Greven, and B. Keimer, *Phys. Rev. Lett.* **111**, 187001 (2013).
⁴⁹ X. Montiel, T. Kloss, and C. Pépin, *Phys. Rev. B* **95**, 104510 (2017).
⁵⁰ T. Kloss, X. Montiel, and C. Pépin, *arXiv:1510.03038* (2015).
⁵¹ A. Abanov, A. V. Chubukov, and J. Schmalian, *Adv. Phys.* **52**, 119 (2003).
⁵² M. R. Norman and C. Pépin, *Rep. Prog. Phys.* **66**, 1547 (2003).
⁵³ A. Chubukov, D. Pines, and J. Schmalian, in *Superconductivity*, edited by K. Bennemann and J. Ketterson (Springer Berlin Heidelberg, 2008).
⁵⁴ P. A. Lee, N. Nagaosa, and X.-G. Wen, *Rev. Mod. Phys.* **78**, 17 (2006).
⁵⁵ E. Gull, O. Parcollet, and A. J. Millis, *Phys. Rev. Lett.* **110**, 216405 (2013).
⁵⁶ S. Sorella, G. B. Martins, F. Becca, C. Gazza, L. Capriotti, A. Parola, and E. Dagotto, *Phys. Rev. Lett.* **88**, 117002 (2002).
⁵⁷ Z. Wang, G. Kotliar, and X.-F. Wang, *Phys. Rev. B* **42**, 8690 (1990).
⁵⁸ C. M. Varma, *Phys. Rev. B* **55**, 14554 (1997).
⁵⁹ S.-C. Zhang, *Science* **275**, 1089 (1997).
⁶⁰ M. A. Metlitski and S. Sachdev, *Phys. Rev. B* **82**, 075128 (2010).
⁶¹ K. B. Efetov, H. Meier, and C. Pépin, *Nat. Phys.* **9**, 442 (2013).
⁶² J. Brinckmann and P. A. Lee, *Phys. Rev. B* **65**, 014502 (2001).
⁶³ T. Das, *Phys. Rev. B* **86**, 054518 (2012).
⁶⁴ X. Montiel, T. Kloss, and C. Pépin, *Europhys. Lett.* **115** (2016).
⁶⁵ S. Benhabib, Y. Gallais, M. Cazayous, M.-A. Méasson, R. D. Zhong, J. Schneeloch, A. Forget, G. D. Gu, D. Colson, and A. Sacuto, *Phys. Rev. B* **92**, 134502 (2015).
⁶⁶ I. M. Vishik, M. Hashimoto, R.-H. He, W.-S. Lee, F. Schmitt, D. Lu, R. G. Moore, C. Zhang, W. Meevasana, T. Sasagawa, S. Uchida, K. Fujita, S. Ishida, M. Ishikado, Y. Yoshida, H. Eisaki, Z. Hussain, T. P. Devereaux, and Z.-X. Shen, *Proc. Nat. Acad. Sci.* **109**, 18332 (2012).
⁶⁷ I. M. Vishik, N. Barišić, M. K. Chan, Y. Li, D. D. Xia, G. Yu, X. Zhao, W. S. Lee, W. Meevasana, T. P. Devereaux, M. Greven, and Z.-X. Shen, *Phys. Rev. B* **89**, 195141 (2014).
⁶⁸ J. M. Kosterlitz and D. J. Thouless, *J. Phys. C: Solid State Phys.* **6**, 1180 (1973).
⁶⁹ J. R. Schrieffer, *Theory of Superconductivity* (Benjamin Reading, MA, 1964).
⁷⁰ T. Strohm and M. Cardona, *Phys. Rev. B* **55**, 12725 (1997).
⁷¹ X. Montiel, T. Kloss, C. Pépin, S. Benhabib, Y. Gallais, and A. Sacuto, *Phys. Rev. B* **93**, 024515 (2016).
⁷² O. Fischer, M. Kugler, I. Maggio-Aprile, C. Berthod, and C. Renner, *Rev. Mod. Phys.* **79**, 353 (2007).

⁷³ P. P. Orth, B. Jeevanesan, R. M. Fernandes, and J. Schmalian, [arXiv:1703.02210](https://arxiv.org/abs/1703.02210) (2017).